AIAA JOURNAL
Vol. 41, No. 2, February 2003

Using Aeroelastic Modes for Nonlinear Panel Flutter at Arbitrary Supersonic Yawed Angle

Xinyun Guo* and Chuh Mei†
Old Dominion University, Norfolk, Virginia 23529-0247

It is commonly accepted that six in vacuo natural modes are needed for converged, limit-cycle oscillations of isotropic rectangular plates exposed to supersonic flow at zero yaw angle to the principle panel length. For isotropic or orthotropic rectangular plates under an arbitrary nonzero yawed supersonic flow, then 36 or 6 × 6 natural modes are needed; for laminated anisotropic rectangular plates even at zero yaw angle, 36 or fewer natural modes are needed. To deal with such a large number of modes is computationally costly for flutter analysis, causing complexity and difficulty in designing controllers for flutter suppression. A thorough examination and understanding of the panel limit-cycle behavior leads to the use of aeroelastic modes for supersonic nonlinear panel flutter analysis. The system equations of motion are formulated first in structural node degrees of freedom. Aeroelastic modes are selected and determined, and the system equations is expressed in the aeroelastic modal coordinates. Limit-cycle amplitudes are then determined using numerical integration. Examples show that the number of modes could be greatly reduced by using aeroelastic modes. For determining limit-cycle oscillations of isotropic or anisotropic composite rectangular plates at zero or an arbitrary yawed flow angle, only two aeroelastic modes are needed; but six to seven aeroelastic modes are needed for designing controllers for flutter suppression.

Nomenclature

$[A]$, $[B]$, $[D]$	=	laminate extension, coupling, and bending stiffness matrices
$[A_x]$, $[A_y]$	=	aerodynamic influence matrices
a, b	=	panel dimensions
C_a	=	aerodynamic damping coefficient
$[G]$	=	system aerodynamic damping matrix
g_a	=	nondimensional aerodynamic damping
h	=	panel thickness
$[K]$	=	system linear stiffness matrix
$[K1]$, $[K2]$	=	system first- and second-order nonlinear stiffness matrices
$[M]$	=	system mass matrix
M_∞	=	freestream Mach number
$[\bar{Q}]$	=	transformed lamina material stiffness matrix
$\{q\}$	=	modal coordinate vector
q_a	=	dynamic pressure
u, v	=	in-plane displacements
V_∞	=	freestream air velocity
w	=	panel deflection
$\{\varepsilon^0\}$	=	in-plane strain vector
$\{\kappa\}$	=	curvature vector
Λ	=	flow yaw angle
λ	=	nondimensional dynamic pressure
λ_0	=	dynamic pressure specified for aeroelastic modes
ρ	=	plate mass density
ρ_a	=	air mass density
$[\Phi_R]$, $[\Phi_L]$	=	matrices of right and left eigenvectors
$\{\phi_r\}$	=	rth right eigenvector
ω_0	=	reference frequency

Received 31 March 2002; revision received 30 July 2002; accepted for publication 19 September 2002.

*Graduate Research Assistant, Department of Aerospace Engineering. Student Member AIAA.

†Professor, Department of Aerospace Engineering; cmei@odu.edu. Associate Fellow AIAA.

I. Introduction

IT is commonly accepted that a minimum of six (or 6 × 1) in vacuo natural modes (NMs) is required for converged limit-cycle oscillations (LCOs) of isotropic rectangular plates at supersonic flow speed at zero yaw angle.[1] It is then expected that 6 × 6 or 36 NMs are needed for isotropic rectangular plates for converged LCOs at an arbitrary yawed supersonic flow.[2] Few investigations on LCO have dealt with yawed airflow. Friedmann and Hanin[3] were the first to study nonlinear flutter of rectangular isotropic or orthotropic panels with arbitrary supersonic flow directions. They used the first-order quasi-steady aerodynamic theory and Galerkin's method with a 4 × 2 or eight NMs (four in the x direction and two in the y direction) model for panels of simply supported edges. Numerical integration was employed for the LCO response. Chandiramani et al.[4,5] used the third-order piston theory aerodynamics and the higher-order shear deformation theory and investigated nonperiodic flutter of a buckled composite panel. The yawing of flow was considered, and Galerkin's method with a 2 × 2 or four NMs model was employed for simply supported rectangular laminated composite panel. The numerical integration was used for quasi-periodic/chaotic flutter motion. For arbitrary laminated anisotropic composite rectangular plates, Abdel-Motagaly et al.[2] have shown that 36 or fewer NMs of the lowest natural frequencies are needed for accurate LCO even at zero yaw angle. An efficient iterative eigensolution procedure was employed for the determination of LCO from the coupled nonlinear modal equations. They have introduced a modal participation value for the selection of those NMs contributing the most to LCO. For nonlinear flutter suppression in controller design, this would certainly cause complexity and difficulty in dealing with such a large number of NMs.[6,7] This leads us to the investigation of whether it is possible to analyze nonlinear panel flutter using some reduced modeling basis with fewer degrees of freedom (DOF), particularly much fewer than the accepted number of NMs. An in-depth examination and through understanding of the solution procedure in determining panel LCO response reveals that it is feasible to use a small number of aeroelastic modes (AEMs) for isotropic and composite rectangular plates at zero or arbitrary flow yaw angle. For fundamental theories and understanding of panel flutter LCO using NMs, see Refs. 8–12.

This paper presents for the first time the analysis of nonlinear flutter of isotropic and composite panels using the AEMs at arbitrary supersonic yawed angle. The classical laminated plate theory is employed for thin composite panels, and the von Kármán nonlinear strain–displacement relations are used for moderately large panel deflections. Quasi-steady first-order piston theory aerodynamics is

employed for the aerodynamic pressure. The system equations of motion are derived and expressed first in structural node DOF. The linear AEMs are selected and determined, and the system equations of motion are transformed in terms of the aeroelastic modal coordinates. Panel LCO responses are determined using an integration scheme for a given combination of flow yaw angle Λ, dynamic pressure λ, and aerodynamic damping C_a. Numerical examples include a square and a rectangular simply supported isotropic plate and a rectangular clamped laminated composite plate to show the accuracy of LCO results attainable in using AEMs. Convergence and selection of the AEMs on LCO are also investigated and presented.

II. Aeroelastic Modes

There are two distinct analysis methods in supersonic nonlinear panel flutter: the time domain and the frequency domain. In time-domain approaches, the coupled nonlinear modal (in NMs) equations are formulated from the governing partial differential equations[1,3–5] in conjunction with Galerkin's method in the spatial domain, or from the finite element modal formulation.[6,7] LCO responses are then determined from the nonlinear modal equations using techniques including numerical integration, harmonic balance, or the perturbation method in the time domain. In frequency-domain approaches, the coupled nonlinear equations of motion are formulated using finite element methods and are expressed in the structural node DOF[13] or natural modal coordinates.[2] The panel responses are determined by an iterative linearized eigensolution using the linearized updated mode with a nonlinear time function (LUM/NTF) approximation.[2,13–15]

When the frequency-domain method in NMs (Fig. 1) is used for a simply supported isotropic square plate at $\Lambda = 0$ deg, the six in vacuo NMs, modes (1, 1)–(6, 1), used in the analysis are located on the vertical axis at $\lambda = 0$. The linear ($W_{\max}/h = 0.0$) eigenvalues for modes (1, 1) and (2, 1) coalesce at the critical dynamic pressure $\lambda_{cr} = 512$. With the LUM/NTF approximation, the converged iterative linearized eigenvalues κ vs λ for two typical large amplitudes $W_{\max}/h = 0.6$ and 1.2 are shown, and they coalesced at the flutter dynamic pressures λ_{f1} and λ_{f2}, respectively. The variation of LCO amplitude $W_{\max}/h$ vs dynamic pressure is, thus, determined and shown in Fig. 2. The LCO deflections at $W_{\max}/h = 0.6$ and 1.2 are shown in Fig. 3.

Reexamine Fig. 1; the LCO occurs at $\lambda > \lambda_{cr}$, whereas the six base NMs are located far away at $\lambda = 0$. Why does one not consider using the AEMs that reside near the LCO in the K–λ plot of Fig. 1. The AEMs are the linear panel vibration modes under the influence of dynamic pressure $0 < \lambda < \lambda_{cr}$. The lowest two normalized AEMs at $\lambda = 510$ is shown in Fig. 4. By comparison of the LCO deflection shapes in Fig. 3 and the AEMs in Fig. 4, it is now much certain that the use of AEMs will reduce the number of DOF for the limit-cycle analysis because the LCO deflections and the AEMs have great similarities in shape.

The concept of use of multidisciplinary AEMs for multidisciplinary panel flutter problems can be extended to other multidisciplinary fields. The use of vibration modes immersed in water[16] for the design and analysis of offshore platforms and the use of vibration modes[17] at temperature $T >$ critical buckling temperature T_{cr} for structures and machineries operating at elevated temperatures are two examples.

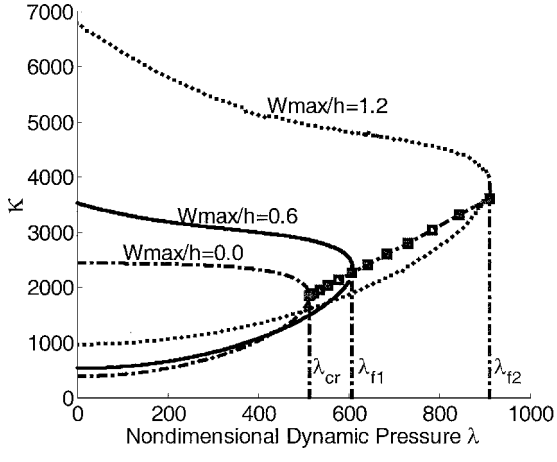

Fig. 1 Eigenvalues K vs dynamic pressure for a simply supported isotropic square plate at $\Lambda = 0$ deg.

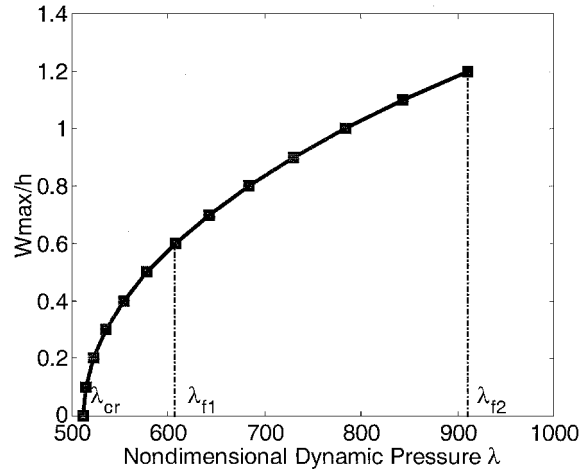

Fig. 2 LCO amplitudes vs dynamic pressure for a simply supported isotropic square plate at $\Lambda = 0$ deg.

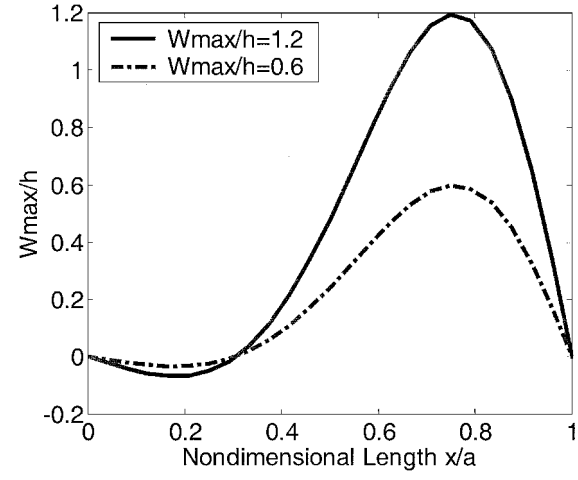

Fig. 3 LCO deflections of $W_{\max}/h = 0.6$ and 1.2 at $y = b/2$ for a simply supported isotropic square plate at $\Lambda = 0$ deg.

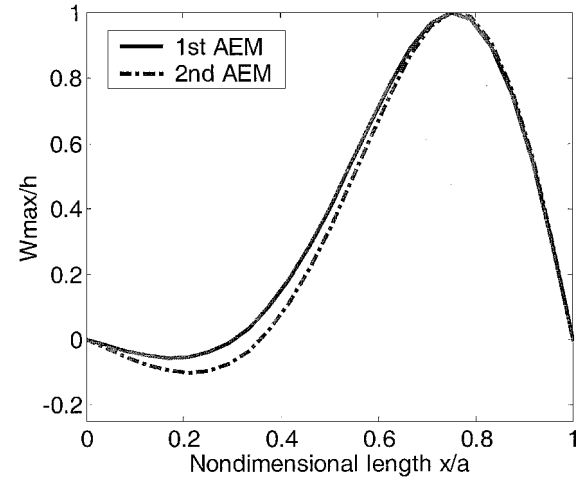

Fig. 4 Normalized AEMs at $\lambda_0 = 510$ for a simply supported isotropic square plate at $\Lambda = 0$ deg.

III. Finite Element Formulation

A. Constitutive Equations

In the derivation of equations of motion, it is assumed that the panel is thin, that is, the ratio of length or width over thickness is

greater than 50. The rotary inertia and transverse shear deformation effects are, thus, negligible. The in-plane strains and curvatures based on von Kármán large deflection and classical laminated plate theories are given by

$$\{\varepsilon\} = \begin{Bmatrix} u_{,x} \\ v_{,y} \\ u_{,y} + v_{,x} \end{Bmatrix} + \frac{1}{2}\begin{Bmatrix} w_{,x}^2 \\ w_{,y}^2 \\ 2w_{,x}w_{,y} \end{Bmatrix} + z\begin{Bmatrix} -w_{,xx} \\ -w_{,yy} \\ -2w_{,xy} \end{Bmatrix}$$

$$= \{\varepsilon_m^0\} + \{\varepsilon_b^0\} + z\{\kappa\} \tag{1}$$

where the subscripts m and b denote membrane (in-plane) and bending components, respectively. For an aircraft panel consisting of fiber-reinforced composite layers, the stress–strain relationships for a general kth layer can be expressed as

$$\begin{Bmatrix} \sigma_x \\ \sigma_y \\ \tau_{xy} \end{Bmatrix}_k = \begin{bmatrix} \bar{Q}_{11} & \bar{Q}_{12} & \bar{Q}_{16} \\ \bar{Q}_{12} & \bar{Q}_{22} & \bar{Q}_{26} \\ \bar{Q}_{16} & \bar{Q}_{26} & \bar{Q}_{66} \end{bmatrix}_k \begin{Bmatrix} \varepsilon_x \\ \varepsilon_y \\ \gamma_{xy} \end{Bmatrix} \tag{2a}$$

or

$$\{\sigma\}_k = [\bar{Q}]_k\{\varepsilon\} \tag{2b}$$

The constitutive relations for a composite laminate are

$$\begin{Bmatrix} N \\ M \end{Bmatrix} = \begin{Bmatrix} A & B \\ B & D \end{Bmatrix}\begin{Bmatrix} \varepsilon^0 \\ \kappa \end{Bmatrix} \tag{3}$$

where the laminate stiffness matrices and stress resultants are

$$([A], [B], [D]) = \int_{-h/2}^{h/2} [\bar{Q}]_k(1, z, z^2)\,\mathrm{d}z \tag{4}$$

$$(\{N\}, \{M\}) = \int_{-h/2}^{h/2} \{\sigma\}_k(1, z)\,\mathrm{d}z \tag{5}$$

B. First-Order Piston Theory Aerodynamics

The quasi-steady first-order piston theory aerodynamics is employed for the aerodynamic pressure. Although this theory neglects the effects of flow memory, it gives a very satisfactory approximation for high supersonic Mach numbers ($M_\infty > 1.6$). The aerodynamic pressure is given by

$$\Delta p = -(2q_a/\beta)\Big\{w_{,x}\cos\Lambda + w_{,y}\sin\Lambda + \Big[\Big(M_\infty^2 - 2\Big)\Big/\Big(M_\infty^2 - 1\Big)\Big](1/V_\infty)w_{,t}\Big\}$$

$$= -\Big[\lambda\Big(D_{110}\Big/a^3\Big)(w_{,x}\cos\Lambda + w_{,y}\sin\Lambda) + (g_a/\omega_0)\Big(D_{110}\Big/a^4\Big)w_{,t}\Big] \tag{6}$$

where Λ is the flow yaw angle with the x axis and the nondimensional dynamic pressure λ and aerodynamic damping g_a are given by

$$\lambda = \frac{2q_a a^3}{\beta D_{110}}, \qquad g_a = \frac{\rho_a V_\infty\Big(M_\infty^2 - 2\Big)}{\rho h\omega_0\beta^3} = \sqrt{\lambda C_a}$$

$$\mu = \frac{\rho_a a}{\rho h}, \qquad C_a = \left(\frac{M_\infty^2 - 2}{M_\infty^2 - 1}\right)^2\frac{\mu}{\beta} \tag{7}$$

and $\beta = \sqrt{(M_\infty^2 - 1)}$, $\omega_0 = (D_{110}/\rho h a^4)^{1/2}$, and D_{110} is the first entry of laminate bending stiffness matrix with all fibers aligned in the x direction supposedly.

C. Equations of Motion

Using Hamilton's principle and finite element expressions, the system equations of motion in structural node DOF for nonlinear panel flutter at an arbitrary flow angle, after assembling the element matrices and considering the kinematic boundary conditions, can be expressed as[2]

$$\frac{1}{\omega_0^2}\begin{bmatrix} [M]_b & 0 \\ 0 & [M]_m \end{bmatrix}\begin{Bmatrix} \ddot{W}_b \\ \ddot{W}_m \end{Bmatrix} + \frac{g_a}{\omega_0}\begin{bmatrix} [G] & 0 \\ 0 & 0 \end{bmatrix}\begin{Bmatrix} \dot{W}_b \\ \dot{W}_m \end{Bmatrix}$$

$$+ \left(\lambda\begin{bmatrix} [A_x]\cos\Lambda + [A_y]\sin\Lambda & 0 \\ 0 & 0 \end{bmatrix} + \begin{bmatrix} [K]_b & [K_B] \\ [K_B]^T & [K]_m \end{bmatrix} + \begin{bmatrix} [K1_{Nm}] + [K1_{Nb}] & [K1]_{bm} \\ [K1]_{mb} & 0 \end{bmatrix} + \begin{bmatrix} [K2] & 0 \\ 0 & 0 \end{bmatrix}\right)\begin{Bmatrix} W_b \\ W_m \end{Bmatrix} = \begin{Bmatrix} 0 \\ 0 \end{Bmatrix} \tag{8}$$

where $[K1]$ and $[K2]$ depend linearly and quadratically on the unknown displacements $\{W\}$. The subscripts B, N_m, and N_b denote that the corresponding stiffness matrix is due to the laminate extension–bending stiffness $[B]$, and membrane force components $\{N_m\}(=[A]\{\varepsilon_m^0\})$ and $\{N_b\}(=[B]\{\kappa\})$, respectively; and subscripts x and y denote that the corresponding aerodynamic influence matrix is due to the $w_{,x}$ and $w_{,y}$ terms in Eq. (6), respectively.

D. Symmetric Laminated Panel

For symmetric composite and isotropic panels, the laminate coupling matrix $[B]$ is null. This leads to

$$[K_B] = [K1_{Nb}] = 0 \tag{9}$$

When the in-plane inertial term is neglected in Eq. (8), the in-plane displacements can be expressed in terms of the bending displacement vector $\{W_b\}$ as

$$\{W_m\} = -[K]_m^{-1}[K1]_{mb}\{W_b\} \tag{10}$$

Thus, the system equation (8) is expressed in terms of the bending displacement $\{W_b\}$ as

$$\Big(1\Big/\omega_0^2\Big)[M_b]\{\ddot{W}_b\} + (g_a/\omega_0)[G]\{\dot{W}_b\} + ([K_L] + [K_{\mathrm{NL}}])\{W_b\} = 0 \tag{11}$$

where the linear and nonlinear stiffness matrices are given by

$$[K_L] = \lambda([A_x]\cos\Lambda + [A_y]\sin\Lambda) + [K]_b = \lambda[A_a] + [K]_b \tag{12}$$

$$[K_{\mathrm{NL}}] = [K1_{Nm}] + [K2] - [K1]_{bm}[K]_m^{-1}[K1]_{mb} \tag{13}$$

Equation (8) or (11) can be solved for nonlinear flutter response in the frequency domain using LUM/NTF approximation. However, using the system equations in the form presented in Eq. (8) or (11) have two disadvantages: 1) The element nonlinear stiffness matrices have to be evaluated and the system nonlinear stiffness matrices must be assembled and updated at each iteration, and 2) the number of structural node DOF of $\{W_b\}$ is usually very large. This turns out to be computationally costly. An efficient solution procedure is to transfer Eq. (11) into the NMs[2,6,7] or even more efficiently the AEMs (present paper).

E. Equations in Aeroelastic Modal Coordinates

Assume that the panel deflection can be expressed as a linear combination of some known base functions as

$$\{W_b\} = \sum_{r=1}^{n} q_r(t)\{\phi_r\} = [\Phi_R]\{q\} \tag{14}$$

where the number of retained linear aeroelastic modes, n, is much smaller than the number of structural node DOF in bending $\{W_b\}$ as well as the number of NMs. The rth AEM $\{\phi_r\}$ is a right eigenvector and normalized with the maximum component to unity as shown in

Fig. 4. The matrix of selected AEMs $[\Phi_R]$, which is the matrix of right eigenvectors, and the corresponding linear frequencies ω_r are obtained from the linear vibration of the system with the influence of aerodynamic influence matrix term

$$\left(\omega_r^2/\omega_0^2\right)[M]_b\{\phi_r\} = ([K]_b + \lambda_0[A_a])\{\phi_r\} \tag{15}$$

where λ_0 is a certain selected dynamic pressure value. The aerodynamic matrix $[A_a]$ is skew symmetric, and thus, the combined matrix $([K]_b + \lambda_0[A_a])$ is nonsymmetrical. Hence, the desirable properties of the eigenvalues and eigenvectors associated with symmetric matrices no longer exist.[18] In particular, for $\lambda_0 < \lambda_{cr}$, the eigenvalues and eigenvectors are real, but the eigenvectors are no longer orthogonal. Here we utilize the concept of right and left eigenvectors[18] to transform the system equations into modal coordinates.

Based on AEMs, it is necessary to transform all of the nonlinear stiffness matrices in Eq. (13) into aeroelastic modal coordinates. Matrices $[K1]_{mb}$ and $[K2]$ are functions of the unknown bending DOF $\{W_b\}$; they can be expressed as the sum of products of AEM coordinates and nonlinear modal stiffness matrices as

$$[K1]_{mb} = \sum_{r=1}^{n} q_r [K1]_{mb}^{(r)} \tag{16}$$

$$[K2] = \sum_{r=1}^{n}\sum_{s=1}^{n} q_r q_s \left([K2]^{(rs)}\right) \tag{17}$$

where the superscripts of those nonlinear modal stiffness matrices denote that they are assembled from the corresponding element nonlinear stiffness matrices. Those element nonlinear stiffness matrices are evaluated with the corresponding element components $\{w_b\}^{(r)}$ obtained from the known system linear AEM $\{\phi_r\}$. Therefore, the nonlinear modal stiffness matrices are constant matrices. The first-order nonlinear stiffness matrix $[K1_{Nm}]$ is a linear function of the in-plane displacement $\{W_m\}$, and from Eq. (10), $\{W_m\}$ consists of the product of two matrices as

$$\{W\}_m = -[K]_m^{-1}\left(\sum_{r=1}^{n} q_r\left([K1]_{mb}^{(r)}\right)\right)[\Phi_R]\{q\}$$

$$= -\sum_{r=1}^{n}\sum_{s=1}^{n} q_r q_s \{\phi_{rs}\}_m \tag{18}$$

where the in-plane mode corresponding to the AEMs $\{\phi_r\}$ and $\{\phi_s\}$ is

$$\{\phi_{rs}\}_m = [K]_m^{-1}[K1]_{mb}^{(r)}\{\phi_s\} \tag{19}$$

Thus, the nonlinear stiffness matrix $[K1_{Nm}]$ can be expressed as the sum of the products of AEM coordinates and nonlinear modal stiffness matrices as

$$[K1_{Nm}] = -\sum_{r=1}^{n}\sum_{s=1}^{n} q_r q_s [K2_{Nm}]^{(rs)} \tag{20}$$

Note that $[K1_{Nm}]$ is quadratic in AEM coordinates. The nonlinear modal stiffness matrix $[K2_{Nm}]^{(rs)}$ is assembled and evaluated with known in-plane mode $\{\phi_{rs}\}_m$, and it is also a constant matrix.

Equation (11) is transformed to the following reduced nonlinear system in the modal coordinates:

$$\left(1/\omega_0^2\right)[\bar{M}_b]\{\ddot{q}\} + (g_a/\omega_0)[\bar{G}]\{\dot{q}\} + ([\bar{K}_L] + [K_{qq}])\{q\} = \{0\} \tag{21}$$

where the modal mass, aerodynamic damping, and linear stiffness matrices are given by

$$([\bar{M}_b], [\bar{G}], [\bar{K}_L]) = [\Phi_L]^T([M_b], [G], [K_L])[\Phi_R] \tag{22}$$

and the cubic term in modal coordinates is

$$[K_{qq}]\{q\} = [\Phi_L]^T \sum_{r=1}^{n}\sum_{s=1}^{n} q_r q_s \Big([K2]^{(rs)} - [K2_{Nm}]^{(rs)}$$

$$- [K1]_{bm}^{(r)}[K]_m^{-1}[K1]_{mb}^{(s)}\Big)[\Phi_R]\{q\} \tag{23}$$

where $[\Phi_L]$ is the matrix of left eigenvectors[18] corresponding to the selected AEMs, which are the selected right eigenvectors. Because the original matrix of left eigenvectors $[\Phi'_L]$ (square matrix) is related with the original matrix of right eigenvectors $[\Phi'_R]$ (square matrix) by $[\Phi'_L]^T = [\Phi'_R]^{-1}$, left eigenvector $[\Phi_L]$ is obtained by extracting the corresponding parts from the $[\Phi'_R]^{-1}$.

F. Time-Domain Solution Procedure

All of the modal matrices in Eq. (21) are constant matrices. In this procedure, the eigenvalue problem of Eq. (15) with selected λ_0 is solved first to generate the AEMs; next, a certain number of AEMs are retained in the finite element modal reduction. With arbitrary given initial conditions and a given set of dynamic pressure λ, flow angle Λ, and aerodynamic damping C_a, the modal amplitude $\{q\}$ can be determined from Eq. (21) using any numerical integration scheme such as the Runge–Kutta or Newmark-β method. The Runge–Kutta method is employed in present paper.

A participation value that evaluates the contribution from the rth AEM to the total deflection is defined as

$$P(r\text{th mode}) = \frac{\max|q_r|}{\sum_{s=1}^{n}(\max|q_s|)} \tag{24}$$

Thus, the minimum number of AEMs for an accurate and converged solution can be determined based on the modal participation values. Because AEMs, unlike natural modes, depend also on the dynamic pressure, the selection of AEMs or λ_0 in Eq. (15) for accurate LCO is studied and presented.

IV. Results and Discussion

To validate the present finite element modal formulation using AEMs, the LCO results for an isotropic square, a rectangular, and a composite rectangular panel are determined and compared with LCO results using the NMs. LCO results at zero flow angle is studied and presented and then followed by nonzero flow angles. The finite element employed in the examples is the four-node Boger–Fox–Schmit (BFS) rectangular plate element.[19] The BFS element has 24 DOF, 6 at each node; the bending DOF, $\{w_b\}$, comprise transverse displacements and first and second derivatives of displacements w, $w_{,x}$, $w_{,y}$, $w_{,xy}$; and the in-plane DOF, $\{w_m\}$, comprise u and v.

Three examples are considered. For the simply supported isotropic square plate at $\Lambda = 0$, a 12×3 mesh or 36 BFS elements in a half plate model is used; at $\Lambda \neq 0$, a 12×12 mesh or 144 BFS elements of the full plate is used. An aerodynamic damping $C_a = 0.01$ is employed. For the simply supported isotropic rectangular plate of $15 \times 12 \times 0.050$ in. ($38.1 \times 30.5 \times 0.127$ cm) at $\Lambda \neq 0$, a 12×12 mesh full plate model is employed. The aerodynamic damping coefficient C_a is set to 0.05. A clamped three-layered $[-40/40/-40]$ rectangular laminate of $15 \times 12 \times 0.048$ in. ($38.1 \times 30.5 \times 0.122$ cm) is investigated. The full plate is modeled with 12×12 mesh or 144 BFS elements for both $\Lambda = 0$ and $\Lambda \neq 0$. The material properties of graphite/epoxy are $E1 = 22.5$ Mpsi (Msi) (155 GPa), $E2 = 1.17$ Msi (8.07 GPa), $G12 = 0.66$ Msi (4.55 GPa), $\gamma 12 = 0.22$, and $\rho = 0.1458 \times 10^{-3}$ lb $\cdot$ s^2/in.^{4} (1550 kg/m^3). The aerodynamic damping coefficient C_a is also set to 0.01.

A. Flow Yaw Angle $\Lambda = 0$ Degree

For the simply supported isotropic square plate, it is known that $\lambda_{cr} = 512$. First, the LCO amplitudes using two AEMs ($\lambda_0 = 510$, Fig. 4) are determined and compared with results using six NMs shown in Fig. 5. The present AE modal formulation gives accurate LCO response. The time history and phase plot of LCO at $\lambda = 890$ are shown in Figs. 6 and 7, respectively.

The convergence of LCO amplitudes using various numbers of AEMs at $\lambda_0 = 510$ is investigated and shown in Fig. 8. It can be seen clearly that the LCO converges fast. It can be also seen in Table 1, which shows the modal participation values for the six AEMs, where the first and second AEMs are dominant. Table 1 also gives the modal participation values for the six NMs. Comparison shows that the method using AEMs converges faster than NMs.

Table 1 Comparison of modal participation values in using six AEMs ($\lambda_0 = 510$) and six NMs for the simply supported isotropic square plate at $\Lambda = 0$ deg

		Modal participation, %					
W_{max}/h	Modes	$q1$	$q2$	$q3$	$q4$	$q5$	$q6$
0.24	AEM	53.18	46.35	0.36	0.05	0.03	0.01
	NM	42.37	41.82	11.87	2.46	1.03	4.31
0.51	AEM	63.93	34.83	0.91	0.21	0.08	0.03
	NM	59.86	30.50	5.96	2.28	0.88	0.46
1.02	AEM	67.32	29.43	1.51	1.16	0.44	0.14
	NM	29.33	45.76	15.23	7.49	0.80	1.38

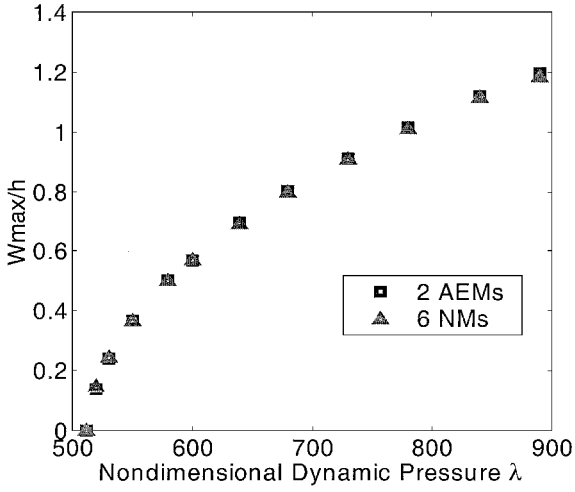

Fig. 5 Comparison of LCO amplitudes using two AEMs and six NMs for a simply supported isotropic square plate at $\Lambda = 0$ deg.

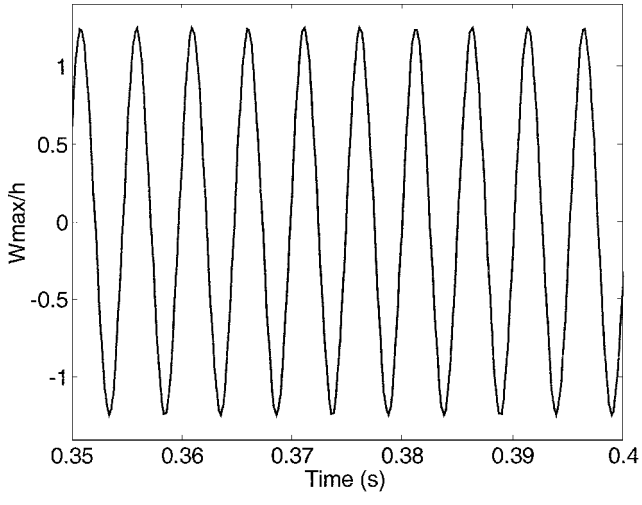

Fig. 6 Time history using two AEMs for a simply supported isotropic square plate at $\lambda = 890$ and $\Lambda = 0$ deg.

One question arises in this procedure: Where should the AEMs be selected? This is because AEMs also depend on dynamic pressure. Intuitively, λ_0 should be selected near the onset of flutter. We know that $\lambda_{cr} = 512$ for a simply supported isotropic square plate. Therefore all of the results obtained (Table 1) are based on AEMs at $\lambda_0 = 510$. To find out the effect of different λ_0 values on LCO results, Fig. 9 shows the difference of LCO amplitudes using two AEMs at three different λ_0 values. The largest difference of LCO amplitudes between $\lambda_0 = 400$ and 510 is about 10%. This indicates that AEMs selection is not very sensitive to LCO results, but the closer to the coalescence λ_{cr}, the more accurate the result will be.

For the clamped rectangular laminated [−40/40/−40] composite plate, we follow the same procedure described earlier. Figure 10 shows the convergence and accuracy of LCO results using 2, 4, and 6 AEMs at $\lambda_0 = 245$ and compared with 36 NMs. The modal participation in Table 2 shows that higher AEMs gradually contributed more at larger limit-cycle amplitudes and that they could not be neglected. The LCO results using two AEMs are good, at least for small amplitudes, but using six AEMs is better for this composite panel.

Table 2 Modal participation values of six AEMs ($\lambda_0 = 245$) for a clamped rectangular laminated composite plate at $\Lambda = 0$ deg

	Modal participation, %					
W_{max}/h	$q1$	$q2$	$q3$	$q4$	$q5$	$q6$
0.22	42.26	47.38	1.21	6.91	1.22	1.00
0.57	40.23	43.88	2.80	8.95	1.34	2.77
1.04	35.42	38.47	7.89	10.38	1.66	6.18

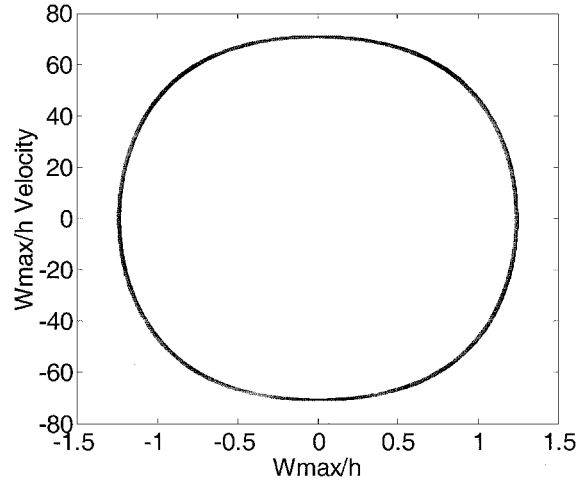

Fig. 7 Phase plot using two AEMs for a simply supported isotropic square plate at $\lambda = 890$ and $\Lambda = 0$ deg.

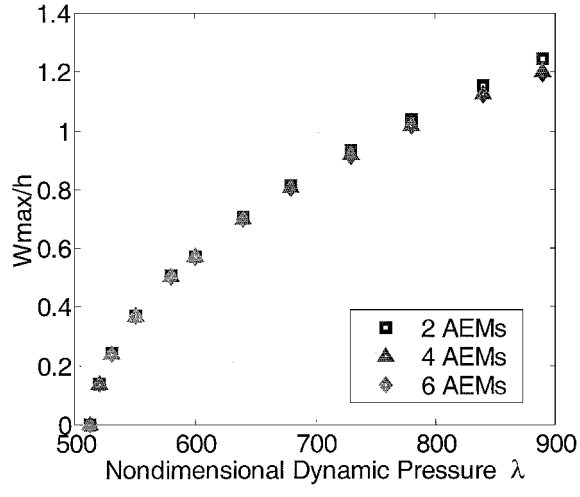

Fig. 8 Convergence of LCO amplitude using AEMs for a simply supported isotropic square plate at $\Lambda = 0$ deg.

B. Flow Yaw Angle $\Lambda \neq 0$ with Method 1

For flow yaw angle $\Lambda \neq 0$, intuitively, we could follow the same procedure as for $\Lambda = 0$. For a particular flow yaw angle, the AEMs are selected and generated with respect to the flow angle, and then the LCO response of the specified flow angle is determined. This means that any other yaw angle cases will follow the procedures just described. This is method 1 for nonlinear panel flutter analysis. In the following, modal convergence and accuracy of LCO results are investigated. Figure 11 shows the LCO amplitudes of the simply supported isotropic square plate at $\Lambda = 15$ deg using 2 and 6 AEMs

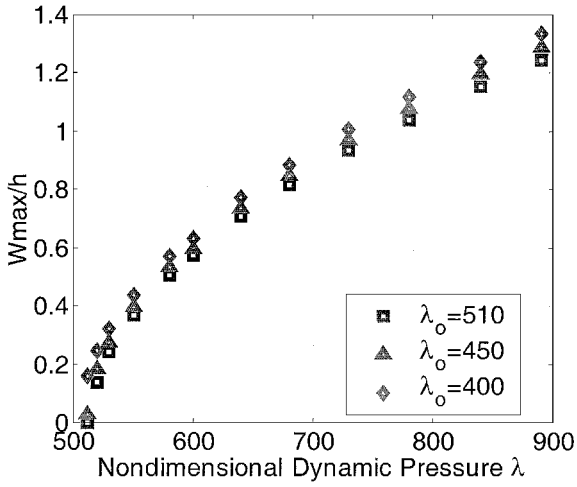

Fig. 9 LCO amplitudes for a simply supported isotropic square plate at $\Lambda = 0$ deg using two AEMs selected at different λ_0.

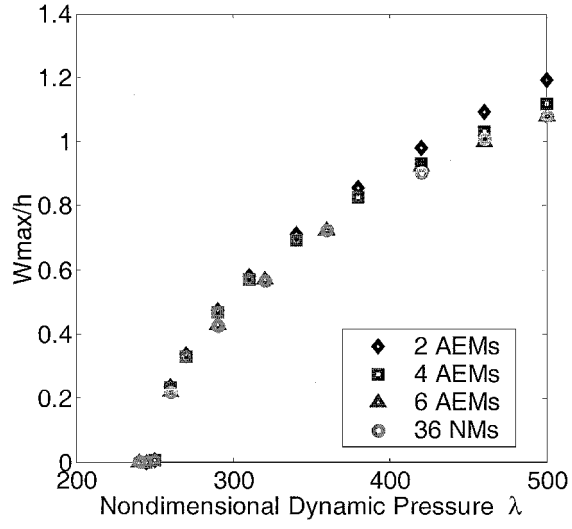

Fig. 10 Comparison of LCO amplitudes using various numbers of AEMs ($\lambda_0 = 245$) and 36 NMs for the clamped rectangular laminated composite plate at $\Lambda = 0$ deg.

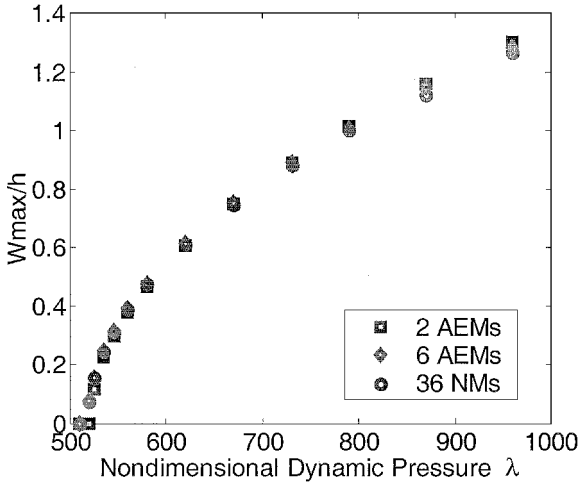

Fig. 11 Comparison of LCO amplitudes using 2 and 6 AEMs ($\lambda_0 = 515$) and 36 NMs for a simply supported isotropic square plate at $\Lambda = 15$ deg (method 1).

Table 3 Modal participation values using six AEMs ($\lambda_0 = 515$) and method 1 for a simply supported isotropic square plate at $\Lambda = 15$ deg

	Modal participation, %					
W_{max}/h	$q1$	$q2$	$q3$	$q4$	$q5$	$q6$
0.08	50.69	48.49	0.04	0.36	0.32	0.09
0.48	60.68	38.23	0.07	0.28	0.53	0.21
1.01	60.32	37.32	0.13	0.64	1.04	0.56

Table 4 Modal participation values for six AEMs ($\lambda_0 = 200$) and method 1 for a clamped rectangular laminated composite plate at $\Lambda = 15$ deg

	Modal participation, %					
W_{max}/h	$q1$	$q2$	$q3$	$q4$	$q5$	$q6$
0.18	51.50	45.90	0.27	1.41	0.24	0.68
0.55	53.93	38.54	0.58	4.55	0.43	1.96
0.96	46.44	38.39	2.52	7.25	0.78	4.61

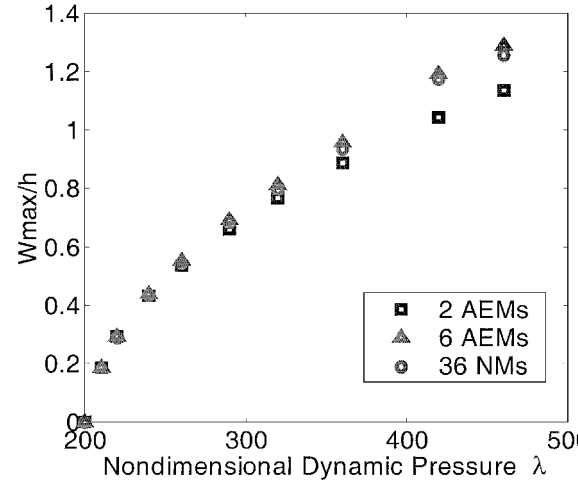

Fig. 12 Comparison of LCO amplitudes using 6 AEMs ($\lambda_0 = 200$) and 36 NMs for a clamped rectangular laminated composite plate at $\Lambda = 15$ deg (method 1).

($\lambda_0 = 515$) compared with using 36 NMs. The results show that even when 2 AEMs are used it is in good agreement with those using 36 NMs. It is seen from Table 3 that the first two AEMs are the most dominant, with all others contributing very little.

For the clamped rectangular laminated composite plate, the results are shown in Fig. 12 and Table 4. Again, it is observed that higher frequency AEMs gradually contribute more at larger amplitudes.

C. Flow Yaw Angle $\Lambda \neq 0$ with Method 2

Method 1 has one disadvantage in controller design for flutter suppression in that it is only for a specified flow angle. This means that the AEMs have to be chosen differently for different flow angles. However, in actual flight, the flow angle could be varied and arbitrary. This makes the controller design much more difficult because it should cover all of the possible flow angles. In another words, it will increase the difficulties greatly if AEMs are considered in flutter suppression. Usually, the controller design technique prefers fewer vibration modes to simplify the control model. For example, piezoelectric patches were studied in control flutter for optimum placements.[6,7] It would be a good idea if a small number of AEMs can be used for all flow angles. Intuitively, evenly distributed AEMs over the range of flow yaw angles can be used for LCO for an arbitrary flow angle.

For the simply supported isotropic square plate, 10 evenly distributed AEMs are first investigated. They are two AEMs at each of the five flow angles $\Lambda = 0$ ($\lambda_0 = 500$), 22.5 ($\lambda_0 = 510$),

Table 5 Modal participation values using six AEMs and method 2 for a simply supported isotropic square plate at $\Lambda = 15$ deg

	Modal participation, %					
W_{max}/h	q_0^1	q_0^2	q_{90}^1	q_{90}^2	q_{30}^1	q_{60}^1
0.25	21.9	28.4	17.3	16.1	13.2	2.94
0.60	26.0	27.6	20.2	20.6	2.21	3.26
1.15	26.3	28.9	20.9	20.7	7.93	2.30

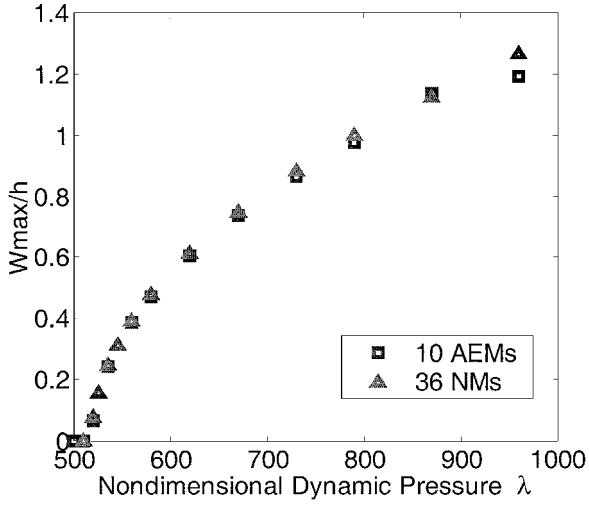

Fig. 13 Comparison of LCO amplitudes using 10 AEMs and 36 NMs for a simply supported isotropic square plate at Λ = 15 deg (method 2).

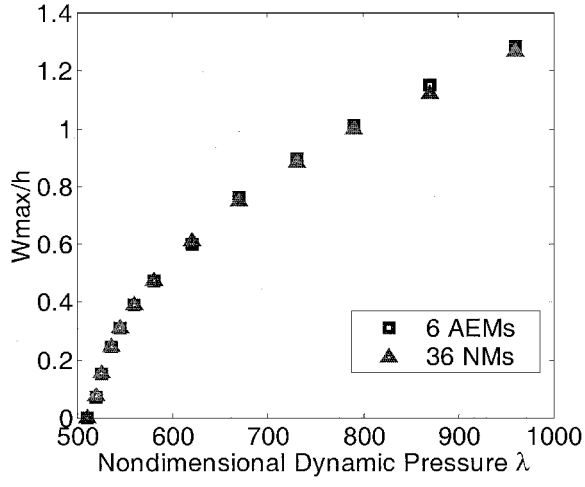

Fig. 14 Comparison of LCO amplitudes at Λ = 15 deg using 6 AEMs and 36 NMs for a simply supported isotropic square plate (method 2).

45 ($\lambda_0 = 514$), 67.5 ($\lambda_0 = 510$) and 90 deg ($\lambda_0 = 500$). Figure 13 shows the comparison of LCO amplitudes with using 36 NMs. To decrease the number of AEMs used, other cases have been investigated. Finally, six AEMs and their locations are determined to be effective: two AEMs q_0^1 and q_0^2 at $\Lambda = 0$ ($\lambda_0 = 510$), two AEMs q_{90}^1 and q_{90}^2 at $\Lambda = 90$ ($\lambda_0 = 510$), one AEM q_{30}^1 at $\Lambda = 30$ ($\lambda_0 = 522$), and one AEM q_{60}^1 at $\Lambda = 60$ deg ($\lambda_0 = 522$). Figure 14 and Table 5 give the results and modal participation values. It is seen that using 6 AEMs has excellent agreement with using 36 NMs for isotropic plate at flow angle $\Lambda = 15$ deg.

For the simply supported isotropic rectangular plate, two flow yaw angles $\Lambda = 15$ and 40 deg are studied, and the aerodynamic damping coefficient C_a is set to 0.05. The six AEMs used are the q_0^1 and q_0^2 at $\Lambda = 0$ ($\lambda_0 = 612$), q_{90}^1 and q_{90}^2 at $\Lambda = 90$ ($\lambda_0 = 867$), the first AEM q_{30}^1 at $\Lambda = 30$ ($\lambda_0 = 656$), and q_{60}^1 at $\Lambda = 60$ deg ($\lambda_0 = 778$). The results are presented in Fig. 15, and the agreement with using 36 NMs is good.

Table 6 Modal participation values at Λ = 15 deg using seven AEMs for the clamped composite rectangular plate

	Modal participation, %						
W_{max}/h	q_0^1	q_0^2	q_{90}^1	q_{90}^2	$q_{22.5}^1$	q_{45}^1	$q_{67.5}^1$
0.18	3.16	0.066	6.63	0.505	20.87	40.50	28.25
0.54	3.39	0.068	6.07	0.463	22.32	40.55	27.12
1.13	3.04	0.079	6.47	0.473	20.47	40.47	27.92

Table 7 Modal participation values at Λ = 60 deg using seven AEMs for the clamped composite rectangular plate

	Modal participation, %						
W_{max}/h	q_0^1	q_0^2	q_{90}^1	q_{90}^2	$q_{22.5}^1$	q_{45}^1	$q_{67.5}^1$
0.17	3.26	0.129	6.05	0.403	21.71	40.64	27.71
0.50	6.50	0.477	1.61	0.215	31.52	41.23	18.32
1.02	3.23	0.068	6.19	0.457	22.13	40.51	27.43

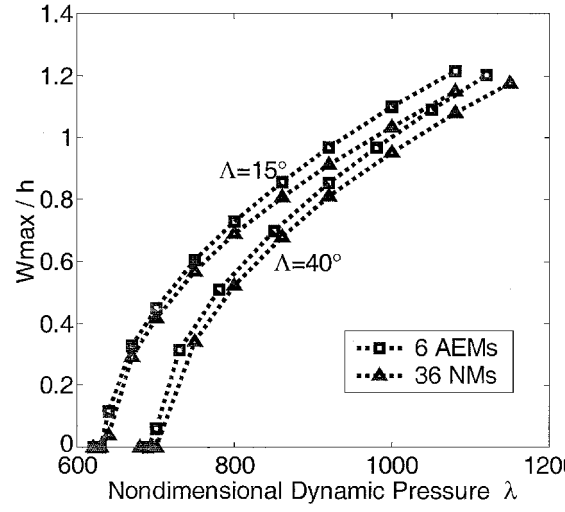

Fig. 15 Comparison of LCO amplitudes using 6 AEMs and 36 NMs for simply supported rectangular isotropic plate at Λ = 15 and 40 deg (method 2).

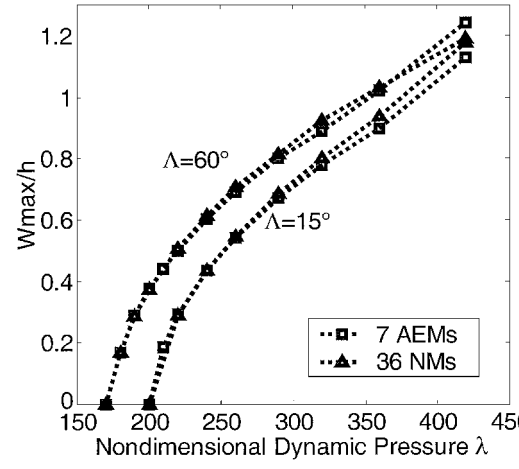

Fig. 16 Comparison of LCO amplitudes at nonzero flow angle for the clamped rectangular composite plate using 7 AEMs and 36 NMs (method 2).

For clamped composite plate, seven AEMs are chosen after some search: q_0^1 and q_0^2, the first and second AEM at $\Lambda = 0$ ($\lambda_0 = 245$); q_{90}^1 and q_{90}^2, the first and second AEM at $\Lambda = 90$ ($\lambda_0 = 218$); $q_{22.5}^1$, the first AEM at $\Lambda = 22.5$ ($\lambda_0 = 186$); q_{45}^1, the first AEM at $\Lambda = 45$ ($\lambda_0 = 168$); and $q_{67.5}^1$, the first AEM at $\Lambda = 67.5$ deg ($\lambda_0 = 176$). LCO amplitudes and modal participation values for yaw angles of 15 and 60 deg are shown in Fig. 16 and Tables 6 and 7. The time history and phase plots of LCO for a yaw angle of 15 deg are also

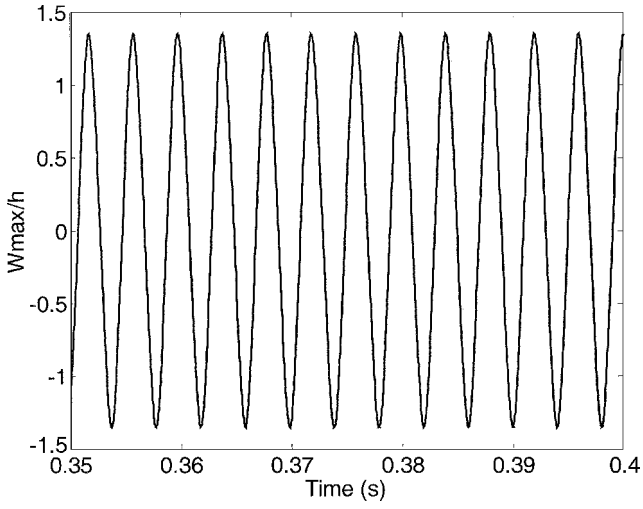

Fig. 17 Time history for the clamped rectangular composite plate using seven AEMs at $\lambda = 460$ and $\Lambda = 15$ deg.

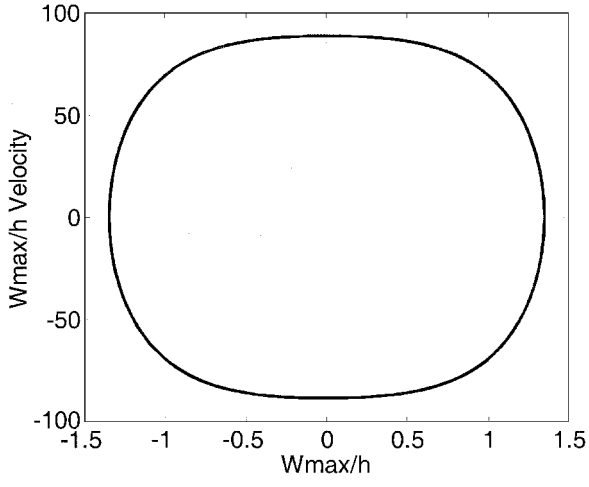

Fig. 18 Phase plot for the clamped rectangular composite plate using seven AEMs at $\lambda = 460$ and $\Lambda = 15$ deg.

presented in Figs. 17 and 18. They all demonstrate that accurate LCO results can be determined with six or seven AEMs. Note that although the modal participation values of q_0^2 and q_{90}^2 are small, they play an role to make the numerical procedures stable.

V. Conclusions

A finite element time-domain formulation using AEMs is presented for the analysis of nonlinear flutter of isotropic and composite panels at arbitrary flow yaw angle. A new and efficient method is presented by introducing the concept of AEMs and using the AE modal transformation to reduce the system equations in structural node DOF to a set of much fewer equations. The method has the advantage of using less computational efforts than other methods and, more important, may provide a much easier base for high-performance panel flutter controller design for flutter suppression. The application of AEMs for converged LCO is studied for isotropic and composite panels with different boundary conditions and at arbitrary flow yaw angles. Results have shown that in using AEMs the number of modal equations can be drastically reduced with little loss in accuracy as compared with those using the NMs. Future work would include applying AEMs on the controller design for flutter suppression and the flutter analysis at elevated temperature environment.

Acknowledgment

The first author would like to acknowledge the support from the Aerospace Engineering Department, Old Dominion University.

References

[1]Dowell, E. H., "Nonlinear Oscillation of a Flutter Plate I," *AIAA Journal*, Vol. 4, No. 7, 1966, pp. 1267–1275.

[2]Abdel-Motagaly, K., Chen, R., and Mei, C., "Nonlinear Flutter of Composite Panels Under Yawed Supersonic Flow Using Finite Elements," *AIAA Journal*, Vol. 37, No. 9, 1999, pp. 1025–1032.

[3]Friedmann, P., and Hanin, M., "Supersonic Nonlinear Flutter of Orthotropic or Isotropic Panels with Arbitrary Flow Direction," *Israel Journal Technology*, Vol. 6, No. 1–2, 1968, pp. 46–57.

[4]Chandiramani, N. K., Plaut, R. H., and Librescu, L., "Nonperiodic Flutter of a Buckled Composite Panel," *Sadhana*, Vol. 20, Pts. 2–4, April–Aug. 1995, pp. 671–689.

[5]Chandiramani, N. K., Plaut, R. H., and Librescu, L., "Nonlinear Flutter of Buckled Shear-Deformable Composite Panel in a High Supersonic Flow," *Journal Nonlinear Mechanics*, Vol. 30, No. 2, 1995, pp. 149–167.

[6]Zhou, R. C., Mei, C., and Huang, J. K., "Suppression of Nonlinear Panel Flutter at Supersonic speeds and Elevated Temperatures," *AIAA Journal*, Vol. 34, No. 2, 1996, pp. 347–354.

[7]Abdel-Motagaly, K., "Finite Element Analysis and Active Control for Nonlinear Flutter of Composite Panels Under Yawed Supersonic Flow," Ph.D. Dissertation, Dept. of Aerospace Engineering, Old Dominion Univ., Norfolk, VA, Dec. 2001.

[8]Dowell, E. H., *Aeroelasticity of Plates and Shells*, Noordhoff International, Leiden, The Netherlands, 1975.

[9]Librescu, L., *Elastostatics and Kinetics of Anisotropic and Heterogeneous Shell-Type Structures*, Noordhoff International, Leiden, The Netherlands, 1975.

[10]Mei, C., Abdel-Motagaly, K., and Chen, R., "Review of Nonlinear Panel Flutter at Supersonic and Hypersonic Speeds," *Applied Mechanics Reviews*, Vol. 52, No. 10, 1999, pp. 321–332.

[11]Bismarck-Nasr, M. N., "Finite Elements in Aeroelasticity of Plates and Shells," *Applied Mechanics Reviews*, Vol. 49, No. 10, Pt. 2, 1996, pp. s17–s24.

[12]Dowell, E. H., "Panel Flutter: A Review of the Aeroelastic Stability of Plates and Shells," *AIAA Journal*, Vol. 8, No. 3, 1970, pp. 385–399.

[13]Xue, D. Y., and Mei, C., "Finite Element Nonlinear Panel Flutter with Arbitrary Temperatures in Supersonic Flow," *AIAA Journal*, Vol. 31, No. 1, 1993, pp. 154–162.

[14]Gray, C. E., Jr., and Mei, C., "Large-Amplitude Finite Element Flutter Analysis of Composite Panels in Hypersonic Flow," *AIAA Journal*, Vol. 31, No. 6, 1993, pp. 1090–1099.

[15]Gray, C. E., Jr., "Large Amplitude Finite Element Flutter Analysis of Composite Panels in Hypersonic Flow," Ph.D. Dissertation, Dept. of Aerospace Engineering, Old Dominion Univ., Norfolk, VA, May 1991.

[16]Lindholm, U. S., Kana, D. D., Chu, W., and Abramson, H. N., "Elastic Vibration Characteristics of Cantilever Plates in Water," *Journal of Ship Research*, Vol. 9, No. 1, 1965, pp. 11–22.

[17]Turner, T. L., "Thermomechanical Response of Shape Memory Alloy Hybrid Composites," NASA TM-2001-210656, Jan. 2001, pp. 105, 109.

[18]Meirovitch, L., *Fundamentals of Vibrations*, McGraw–Hill, New York, 2001, p. 346.

[19]Bogner, F. K., Fox, R. L., and Schmit, L. A., "The Generation of Inter-Element Compatible Stiffness and Mass Matrices by the Use of Interpolation Formulas," AFFDL-TR-66-80, Wright–Patterson AFB, OH, 1966, pp. 396–443.

E. Livne
Associate Editor